UDC 616.7-089.23:519.876

NOT PUBLISHED: DEVELOPMENT OF A LIGHTWEIGHT ABDUCTION SPLINT FOR PEDIATRIC DDH PATIENTS THROUGH TOPOLOGICAL OPTIMIZATION

**Alex Condori Lopez, Eber Mejia Tola, Yuri Silva Vidal,
Erick Valdeiglesias Flores, Daniela Ponte Lopez, Trunks Vasquez Llave**

The object of the study is the structural geometry of an abduction splint for pediatric patients with developmental dysplasia. The problem to be solved is the existing commercial orthotic devices exhibit excessive weight and inadequate contact pressure distribution, leading to soft tissue damage, skin irritation, and poor therapeutic compliance in pediatric patients. Main scientific results – topological optimization based on the solid isotropic material with penalization method was applied to redesign the splint geometry. Three medical-grade polymers (ABS medical, PETG medical, and PP) were comparatively evaluated through static finite element analysis (FEA). ABS Medical was selected as the optimal material due to its initial safety factor of 14.95. The iterative optimization process, spanning 81 cycles, achieved a mass reduction of 18.96% (from 395.34 g to 320.38 g) while maintaining a safety factor of 13.69, significantly exceeding the Pugsley-derived minimum of 2.52 established for pediatric medical devices. Peak contact pressure reached 0.962 kPa, well below the critical 5.2 kPa capillary occlusion threshold. Interpretation – weight reduction results from the redistribution of material along principal stress vectors identified through finite element analysis. Distinctive features – the approach achieves nearly double the mass reduction of comparable studies (18.96% vs. 9.58%). Practical value – these results provide a validated framework for manufacturing lightweight and safer orthopedic devices via fused deposition modeling (FDM) additive manufacturing, minimizing dermatological complications

Keywords: dysplasia, abduction splint, optimization, finite element analysis, additive manufacturing, pediatric

1. Introduction

Developmental dysplasia of the hip (DDH) is a congenital and hereditary musculoskeletal condition characterized by an abnormality in the formation of the hip joint, which can manifest as acetabular dysplasia or hip dislocation. This condition is highly prevalent in newborns [1]. Approximately 2.6 million babies born each year worldwide are diagnosed with hip dysplasia [2, 3]. A systematic review and meta-analysis of 65 studies reported a higher risk in girls [1]. The severity is classified using ultrasonographic techniques into four types: type I (normal hip), type II (mild to moderate dysplasia, the most common), type III, and type IV (dislocation) [4, 5].

If not treated promptly, this condition causes damage to the soft cartilage of the hip joint, increasing the likelihood of developing osteoarthritis [6]. DDH is responsible for up to 50% of cases of degenerative osteoarthritis in adults, affecting patients' quality of life and causing complications such as lameness, chronic pain, and

contractures in the lumbar region [7]. Early treatment is essential to avoid these complications. Orthopedic devices are classified as dynamic and static [8, 9]:

– dynamic devices, such as the Pavlik harness, Frejka pillow, and Tübingen splint, are first-line treatments before 5–6 months of age and offer high efficacy [10–13].

– static devices, such as the Rhino splint, Ilfeld, and abduction splints, are indicated when dynamic devices fail or in more severe dysplasias [11, 14, 15].

The harness is the gold standard in the first months of treatment [9, 12]. However, in patients who do not achieve the expected results, abduction splints or surgery are used. Previous studies [16] demonstrate high effectiveness of abduction splints in type II and even type III dysplasias, positioning them as a viable alternative to dynamic devices [17], with advantages in ease of use for caregivers, although their rigidity and weight remain as limitations.

Despite their efficacy, abduction splints frequently cause skin lesions [18] that can evolve into pressure ulcers or bedsores [19]. Study conducted with caregivers [20] highlights concerns about discomfort and skin irritation, factors that contribute to therapeutic non-compliance and increase the risk of treatment failure [8, 20].

In response to these ergonomic limitations, topological optimization techniques have gained relevance in medical device design, with growing application in orthopedics and rehabilitation [21]. Examples include the design of personalized wrist splints [22], orthoses for fractures with mass reductions of up to 9.58% [23], and anthropomorphic prosthetic devices [24], all focused on reducing weight, improving pressure distribution, and increasing comfort without compromising structural integrity.

Despite these proven advances in various orthopedic applications, topological optimization has not yet been applied to the redesign of abduction splints for DDH treatment. Given the high prevalence of this condition, the documented ergonomic limitations of current devices, and the demonstrated potential of optimization techniques in similar applications, study focused on the development of optimized abduction splints that reduce mass and improve pressure distribution while maintaining structural integrity is relevant for improving treatment outcomes in pediatric patients.

2. Literature review and problem statement

The paper [1] presents the results of the study on risk factor identification in developmental dysplasia of the hip (DDH), analyzing 3,720 children. It is shown that 91.9% of cases had at least two associated risk factors, such as breech presentation and traditional swaddling [1, 6]. But there were unresolved issues related to the generalizability of these findings beyond European populations. The reason for this may be objective difficulties associated with the cost and complexity of conducting large multicenter cohort studies across diverse ethnic groups.

The paper [2] from the Global Hip Dysplasia Registry provides a comprehensive assessment of the global epidemiological impact and the long-term clinical burden of developmental dysplasia of the hip (DDH). It is shown that between 1 and 3 infants per 1,000 live births are diagnosed with a dislocated hip, while hip instability affects approximately 20 per 1,000, leading to an estimated 2.0 to 2.6 million infants affected

annually worldwide. The study also highlights the severe socioeconomic consequences of the condition, noting that DDH is the underlying cause for 28.8% of all total hip replacements performed in patients under 60 years of age.

But there were unresolved issues related to the extreme variability in reported incidence, which fluctuates between 0.06 and 76.1 per 1,000 based on the geographical region and the specific diagnostic criteria applied. Additionally, many prevalence reports are limited by methodological heterogeneity and a lack of high-quality primary studies, which complicates the establishment of a truly accurate global average. The reason for this may be objective difficulties associated with the lack of international consensus on screening protocols and the significant financial and logistical barriers to implementing universal ultrasound programs, which remain a major public health and socioeconomic problem in many regions

The paper [3] presents the results of the study on global DDH prevalence through a comprehensive systematic review and meta-analysis involving 3,451,682 infants across 65 studies. It is shown that the pooled prevalence of DDH is approximately 1.40% (or one in every 100 infants), with girls facing a significantly higher risk than boys (1.46% vs. 0.66%). The study also identifies that while the prevalence of specific hip dysplasia has trended downward, the overall prevalence of DDH has shown a slight upward trend over the last three decades. But there were unresolved issues related to the quality and geographic representativeness of the data, as none of the 65 studies analyzed were classified as "high quality" and a disproportionate 77% of the study originated from China, potentially biasing the "global" average. Furthermore, the exclusion of studies in languages other than English and Chinese may have resulted in the omission of vital epidemiological data from other high-incidence regions. The reason for this may be objective difficulties associated with the high heterogeneity between studies (I^2 = 100%) and the lack of international standardization in screening techniques and clinical criteria, which makes it challenging to synthesize data across diverse healthcare settings and ethnicities.

The papers [4, 5] present the results of the study on diagnostic standardization. It is shown that static ultrasound is the gold standard for infants under six months, using alpha and beta angle measurements to reduce invasive surgery rates by up to 50% [4]. But there were unresolved issues related to the feasibility of universal screening in developing regions. The reason for this may be cost constraints regarding ultrasound infrastructure and specialist training, making universal screening impractical in low-income healthcare systems.

The paper [10] presents the study on the comparative efficacy of orthotic devices. It is shown that dynamic devices like the Pavlik harness are the first line of treatment, while static devices like abduction splints are indicated for severe cases or when dynamic systems fail, achieving up to 82% success in resistant hips [11, 14, 15]. But there were unresolved issues related to the absence of standardized transition criteria between device categories.

The paper [11] presents the results of the study on the clinical impact of hip dysplasia in adults and the efficacy of periacetabular osteotomy (PAO), analyzing 62 studies involving 8,222 participants. It is shown that preoperative patients experience

significantly higher levels of pain (SMD – 4.05) and a lower quality of life (SMD – 4.10) compared to healthy individuals, and while PAO leads to substantial improvements in pain and function – maintained for up to 7 years – patients consistently fail to reach the functional levels of a healthy population. The study also identifies that a history of failed hip arthroscopy correlates with poorer early outcomes after PAO, while the severity of dysplasia (mild vs. severe) does not significantly influence postoperative pain or function.

The papers [13, 16] present study on treatment outcomes and complications. It is shown that while the Tübingen splint achieves 91–98% success with low risks of avascular necrosis (AVN), the Pavlik harness presents AVN risks up to 30% in failed reductions [16]. Furthermore, short-term success does not always prevent residual dysplasia [13]. But there were unresolved issues related to biomechanical limitations that lead to device failure. The reason for this may be objective difficulties associated with current designs that do not account for individual anatomical variability.

The paper [14] presents the results of the study on the short- and intermediate-term outcomes of dislocated hips in infants who failed initial Pavlik harness therapy, analyzing 50 infants (66 hips) treated between 2000 and 2018. It is shown that initiating Pavlik harness treatment after 3 weeks of age and the presence of unilateral dislocations are significant risk factors that increase the likelihood of needing an operating room for reduction. Furthermore, while closed reduction (CR) remains possible in 86.3% of these cases, the study identified a statistically significant association between open reduction and the development of avascular necrosis (AVN), reporting an overall AVN rate of 10.5% in patients who failed Pavlik therapy compared to only 1.0% in those who were successfully treated with the harness.

The paper [15] presents the results of the study on orthosis treatment for congenital hip dislocation in a developing nation context, analyzing 48 patients treated at two major orthopedic centers in Madagascar. It is shown that favorable therapeutic outcomes with successful femoral head recentration were achieved in 79.2% of cases, primarily utilizing abduction pants as the first-line treatment (60.4%) starting at a mean age of 7.8 months. The study highlights that this approach is economically accessible for the local population and, notably, reported zero cases of avascular necrosis (AVN) of the femoral head among the treated cohort.

The paper [17] presents the results of the study on the efficacy and safety of a custom-made abduction brace for the treatment of DDH, analyzing 40 dysplastic hips in 33 infants under 6 months of age. It is shown that the device achieved a successful hip reduction rate of 85%, including a 100% success rate for unilateral Graf types IIa, IIb, and IIc, with no reported cases of avascular necrosis (AVN) or major skin lesions. The study also identifies that the brace's design, which uses flexible Plastazote foam to allow some limb mobility, provides a simpler and more comfortable therapeutic procedure for parents compared to the complex adjustments required by the Pavlik harness.

The paper [20] presents the study on caregiver experiences, showing that devices cause significant concerns regarding child discomfort and skin irritation. But there were unresolved issues related to the physical causes of this discomfort, as the study relied on subjective perception rather than objective biomechanical measurements.

The papers [18, 19] present the study on the consequences of inadequate pressure distribution. It is shown that abduction splints frequently cause skin lesions that can progress to ulcers, especially when pressures exceed the 5.2 kPa capillary closing threshold [23, 24]. But there were unresolved issues related to the absence of design methodologies that systematically reduce pressure while maintaining integrity. The reason for this may be a fundamental impossibility within conventional design approaches, which rely on uniform material thickness and cannot identify optimal regions for material removal.

A way to overcome these difficulties can be the application of topological optimization (TO) based on the solid isotropic material with penalization (SIMP) method combined with additive manufacturing [18, 22]. The paper [21] presents the results of the study on the integration of topological optimization (TO) within the digital manufacturing chain for customized orthopedic devices, specifically focusing on the production of a personalized wrist splint via fused deposition modeling (FDM). It is shown that the TO application allows for a structured reduction in material usage while maintaining or enhancing the device's mechanical performance, resulting in orthoses that are significantly lighter and more ergonomic compared to those designed through traditional experience-based methods. Furthermore, the study identifies that integrating 3D scanning with TO enables a precise anatomical fit that improves both patient comfort and the breathability of the device through the strategic creation of voids. This approach was used in [22] for wrist splints and in [23] for fracture orthoses, achieving a 9.58% mass reduction; however, these studies either lacked reported quantitative data or failed to validate contact pressure distribution. The paper [24] presents the results of the study on the development of a bioinspired, anthropomorphic prosthetic foot for lower limb replacement using topology optimization (TO) and gyroid lattice geometries. It is shown that the integration of 3D scanning with a novel TPU-GTR composite material allows for a unified stress distribution that accurately mimics human locomotion and landing mechanics. The study identifies that a design with 40% relative density is structurally optimal, capable of tolerating forces up to 8,000 N (providing a factor of safety of 1.5) while maintaining a damping factor of 0.18, which is ideal for reducing discomfort and preventing muscle atrophy in other joints. All this allows to conclude that it is expedient to conduct study devoted to the application of topological optimization for the redesign of abduction splints. The literature review has established that:

1) DDH affects millions of infants, requiring high-compliance orthotic treatment [2, 3];

2) current splints have ergonomic limitations, specifically excessive weight and poor pressure distribution [18–20];

3) these flaws lead to skin lesions and therapeutic failure [11, 20];

4) TO has shown success in other devices but has not been applied to DDH splints [21–24].

Therefore, the unresolved problem consists in the absence of optimized abduction splint designs that minimize mass and contact pressure through the SIMP method and medical-grade additive manufacturing.

3. Aim and objectives of the study

The aim of this study is to develop an optimized abduction splint for pediatric patients with developmental dysplasia.

To achieve this aim, the following objectives were accomplished:

– to calculate the biomechanical forces acting on the abduction splint based on pediatric anthropometric data;

– to design the mechanical structure of an abduction splint through reverse engineering of a commercial device;

– to determine the minimum safety factor using Pugsley methodology for pediatric medical devices;

– to perform comparative static finite element analysis of three medical-grade materials suitable for fused deposition modeling;

– to execute topological optimization using the solid isotropic material with Penalization method to minimize mass while maintaining structural safety requirements.

4. Materials and methods

4. 1. The object and hypothesis of the study

The object of the study is the structural geometry of an abduction splint for pediatric patients with developmental dysplasia. The hypothesis that applying the solid isotropic material with penalization (SIMP) method to its load-bearing components will achieve a significant reduction in mass and contact pressure without compromising the minimum safety factor established by Pugsley methodology for pediatric medical devices. Prior to the study, it was assumed that the reference patient is a 7-month-old female infant weighing 7.6 kg per World Health Organization (WHO) growth curves, that applied loads are static and derived from lower limb weight in the critical horizontal position, that the selected medical-grade polymers exhibit linear elastic, isotropic, and homogeneous behavior, and that the reverse-engineered geometry is representative of devices currently used in clinical practice. During the process of the study, dynamic loads from infant movement were not considered given that the static horizontal position represents the worst-case structural scenario, the splint-tissue interaction was modeled as rigid contact without friction, and the mechanical properties of the materials correspond to manufacturer-reported values under standard conditions, not accounting for anisotropy or variability introduced by the FDM printing process.

The methodology combines biomechanical analysis, finite element simulation (FEA), and structural optimization, organized into five components:

1) calculation of acting forces;

2) mechanical design through reverse engineering;

3) structural safety factor calculation;

4) comparative static analysis of biocompatible materials;

5) execution of the topological optimization study.

4. 2. Clinical requirements and anthropometric data

The design parameters were defined based on patients under the age of one, specifically infants aged 6 to 12 months, as this age range represents the critical period for orthotic treatment of developmental dysplasia of the hip (DDH) [9, 10, 12, 13].

The fundamental clinical requirements to ensure treatment efficacy are:

– therapeutic angles: maintenance of the reduction position with an alpha angle > 60° and beta angle < 55° according to Graf's technique [4, 25, 26];

– dermal safety: materials must comply with ISO 10993 standard, which guarantees they are hypoallergenic and biocompatible for prolonged contact with infant skin;

– injury prevention: maximum contact pressure must be below 5.2 kPa to avoid the risk of bedsores or necrosis [20, 23, 24].

4. 3. Material selection

The analyzed materials included: ABS Medical with elastic modulus of 1.40 GPa, yield strength of 46 MPa and density of 1.06 g/cm^3; PETG Medical with elastic modulus of 2.20 GPa, yield strength of 37 to 39 MPa and density of 1.27 g/cm^3; and Polypropylene (PP) with elastic modulus of 0.62 to 0.67 GPa, yield strength of 18 to 20 MPa and density of 0.90 g/cm^3.

4. 4. Load calculation and structural analysis

Biomechanical forces acting on the abduction splint were calculated based on pediatric anthropometric data. The total body weight force was determined from World Health Organization growth curves, and the force generated by each leg was calculated considering that the lower limb represents 16% of total body weight according to anthropometric references [27]. The moment on the femoral head was calculated using anatomical reference points for anthropometric measurements.

Numerical simulation was performed using SolidWorks Simulation (software (Dassault Systèmes, France), applying the Von Mises failure criterion for stress analysis. The safety factor was calculated as the ratio between material yield strength and Von Mises equivalent stress. Two loading positions were analyzed: vertical and horizontal, to identify the critical load case for design validation.

The finite element model assumed linear elastic, isotropic, and homogeneous material behavior for all polymeric components. Contact between the splint and the soft tissue surface was modeled as rigid, frictionless contact, applying the calculated distributed loads directly to the corresponding contact faces. Boundary conditions were defined as fixed constraints at the pelvic support attachment points. Mesh convergence was verified by comparing results across successive refinement levels until the variation in maximum Von Mises stress remained below 2%.

4. 5. Minimum safety factor calculation according to Pugsley tables

To determine the appropriate minimum safety factor for the abduction splint, Pugsley tables were applied. This method allows selecting a realistic safety factor value considering five specific characteristics of the design and its clinical

application: material quality (A), applied load control (B), stress analysis accuracy (C), user hazard (D), and economic impact (E). The method establishes the minimum safety factor through the product of factors associated with these characteristics, with an additional correction factor applied for pediatric medical devices.

The rating of "fair" for material quality (characteristic A) reflects the use of commercial medical-grade polymers with manufacturer-certified mechanical properties, which are subject to batch-to-batch variability and process-induced anisotropy inherent to fused deposition modeling. This qualitative judgment is consistent with Pugsley's classification criteria and translates directly into the n_{xx} factor through the lookup table shown in Fig. 7, thereby propagating the material uncertainty into the minimum safety factor through equation (6).

4. 6. Topological optimization using solid isotropic material with penalization method

The solid isotropic material with penalization method was implemented for topological optimization. This method assigns a density variable to each finite element, ranging from zero (void) to one (solid material), with a penalization exponent that forces intermediate densities to converge toward discrete values. The objective function minimizes structural compliance (maximizes stiffness) subject to a volume fraction constraint. The optimization was performed using SolidWorks Simulation with a penalization exponent of three, iterating until convergence was achieved.

5. Results of topological optimization of abduction splint for developmental dysplasia of the hip treatment

5. 1. Biomechanical forces calculation based on pediatric anthropometric data

Anthropometric data from a 7-month infant were used. Table 1 presents the anthropometric measurements.

Table 1
Anthropometric measurements of the reference patient

Parameter	Value
Thigh length (mm)	150
Thigh circumference (mm)	200
Hip width (mm)	135

Based on a total patient weight of 7.6 kg, obtained from the World Health Organization growth curves (Fig. 1), the total body weight force was calculated as

$$F = m \times g = 7.6 \times 9.81 = 74.56 \text{ N}. \quad (1)$$

According to anthropometric data, the lower limb represents 16% of total body weight [27]. Table 2 shows the body segment weight distribution table used for force calculations.

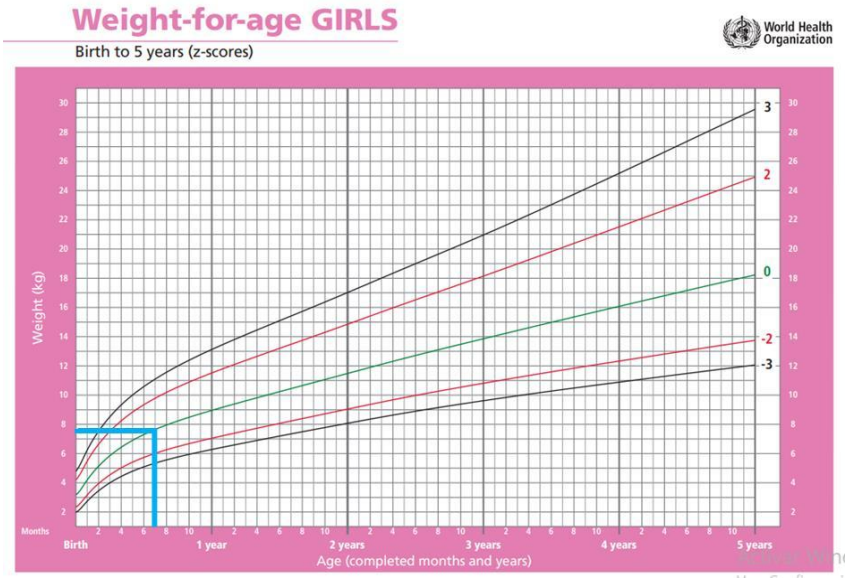

Fig. 1. World Health Organization weight-for-age growth curve for girls (birth to 5 years) used to determine the reference patient weight of 7.6 kg at 7 months of age

Table 2
Body segment weight distribution

Upper limb	Lower limb
Hand = 0.7%	Foot = 1.5%
Forearm and hand = 2.3%	Leg and foot = 5.9%
Upper limb = 5.0%	Lower limb = 16%
Supracondylar = 9.7%	Infracondylar = 4.5%

Therefore, the force generated by one leg is

$$F_{leg} = 74.56 \times 0.16 = 11.93 \text{ N}. \quad (2)$$

The moment on the femoral head was calculated considering the anatomical reference points shown in the Table 3 and Fig. 2

$$M = 11.93 \times 0.15 = 1.79 \text{ Nm}. \quad (3)$$

Table 3
Approximate hip dimensions of 7-month-old female patients

N°	Measurement description	How to take the measurement	Value
I	Hip width	Distance between greater trochanters	16.50 cm
	Hip circumference	At the level of the greater trochanters	46.00 cm
J	ASIS-ASIS distance	Between anterior iliac spines	17.50 cm
	ASIS-ASIS circumference	At the level of the anterior iliac spines	47.50 cm
K	Trochanter-knee length	For lever arm calculation	15 cm
L	Trochanter-ankle length	For limb mass calculation	26 cm

These anthropometric measurements establish the geometric parameters for splint dimensioning and biomechanical calculations. The trochanter-knee length of 15 cm was used as the lever arm for moment calculations, while hip width and ASIS-ASIS distance defined the transverse dimensions of the pelvic support section.

The free body diagram was established with forces F1, F2, F3, moments M2, M3 acting on the splint structure and reactions R1, R2, R3, as shown in Fig. 3.

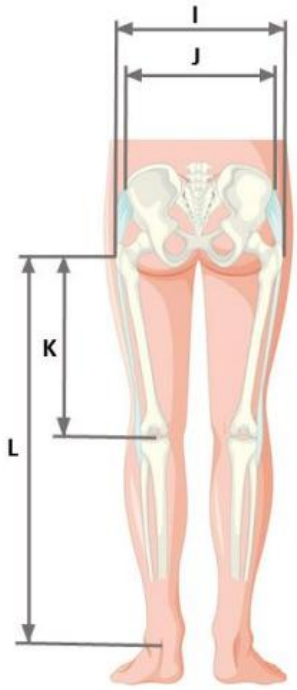

Fig. 2. Anatomical reference points: I – hip width (distance between greater trochanters); J – ASIS-ASIS distance; K – trochanter-knee length; L – trochanter-ankle length

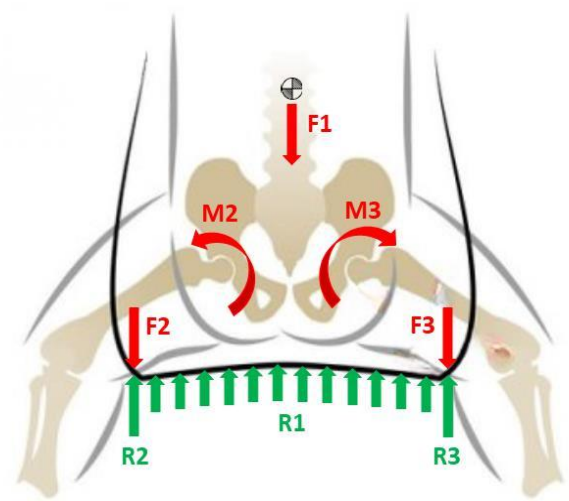

Fig. 3. Free-body diagram: F1– resultant pelvic load; F2, F3 – applied forces on leg supports; M2, M3 – hip abduction moments; R1 – distributed reaction force on the base; R2, R3 – concentrated lateral reactions

These results establish that a 7-month infant generates forces of 11.93 N per leg and moments of 1.79 Nm on the abduction splint structure, providing the load conditions required for subsequent finite element analysis.

5. 2. Mechanical design of the abduction splint through reverse engineering

The abduction splint was designed through reverse engineering of a commercial device. Fig. 4 shows the computer-aided design model of the splint structure with its main components.

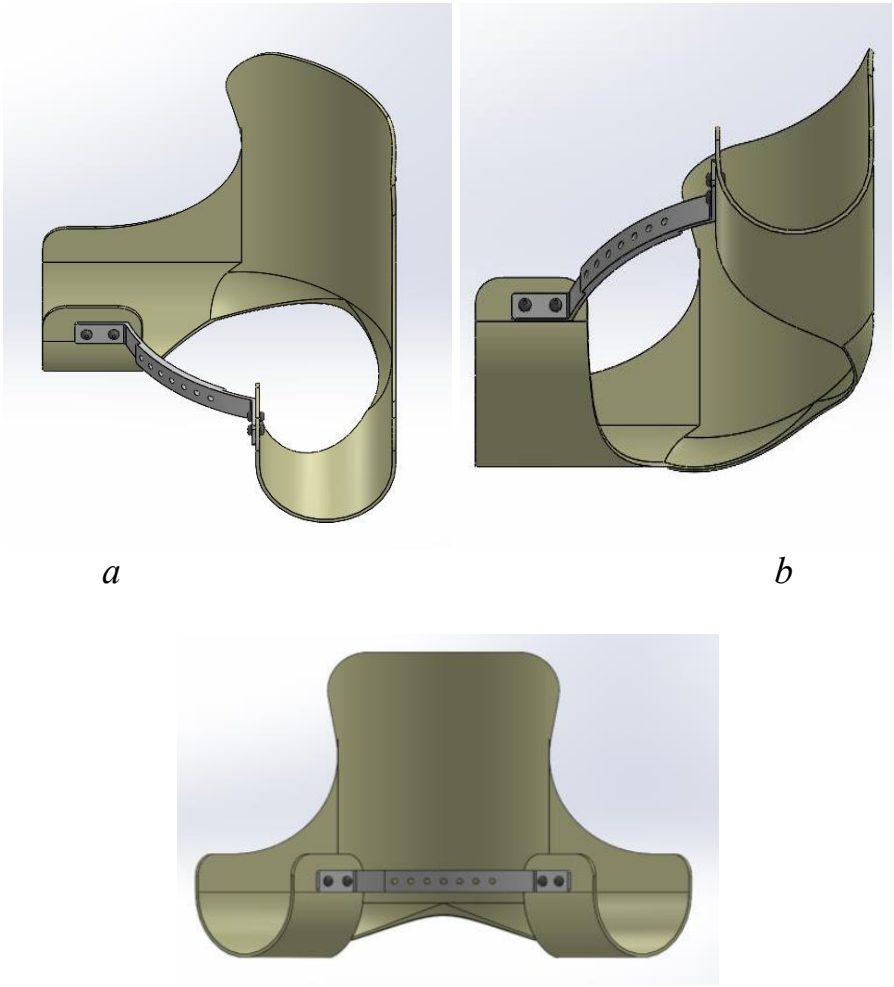

a *b*

c

Fig. 4. CAD model of the abduction splint: *a* – isometric view showing leg support and pelvic section; *b* – side view showing curvature for leg support; *c* – front view showing bilateral leg supports and adjustment bar

The specific materials selected for the baseline SolidWorks Simulation are detailed in Table 4.

The weight of this structure is 406.56 grams. Numerical simulation was performed using SolidWorks Simulation, applying the Von Mises failure criterion

$$\sigma_{VM} = \sqrt{\left[\left(\sigma_1 - \sigma_2\right)^2 + \left(\sigma_2 - \sigma_3\right)^2 + \left(\sigma_1 - \sigma_3\right)^2\right] / 2.} \quad (4)$$

Table 4
SolidWorks simulation materials for commercial abduction splint

Component	Material
Splint structure	Polypropylene copolymer
Aluminum bar	Aluminum 6061-T6
Hardware	Stainless steel AISI 304

The safety factor was calculated as

$$FS = \sigma_{yield} / \sigma_{VM}. \quad (5)$$

Finite element simulation of structural resistance and deformation was performed by applying the calculated loads in two positions. Fig. 5 shows the results for the vertical position.

The weight of this structure is 406.56 grams. Next, in Fig. 5, finite element simulation of structural resistance and deformation was performed by applying the calculated loads.

Then the other possible scenario is when the splint is in horizontal position as shown in Fig. 6, resulting in safety factor values of SF = 9.647 and maximum deformation of 1.251 mm.

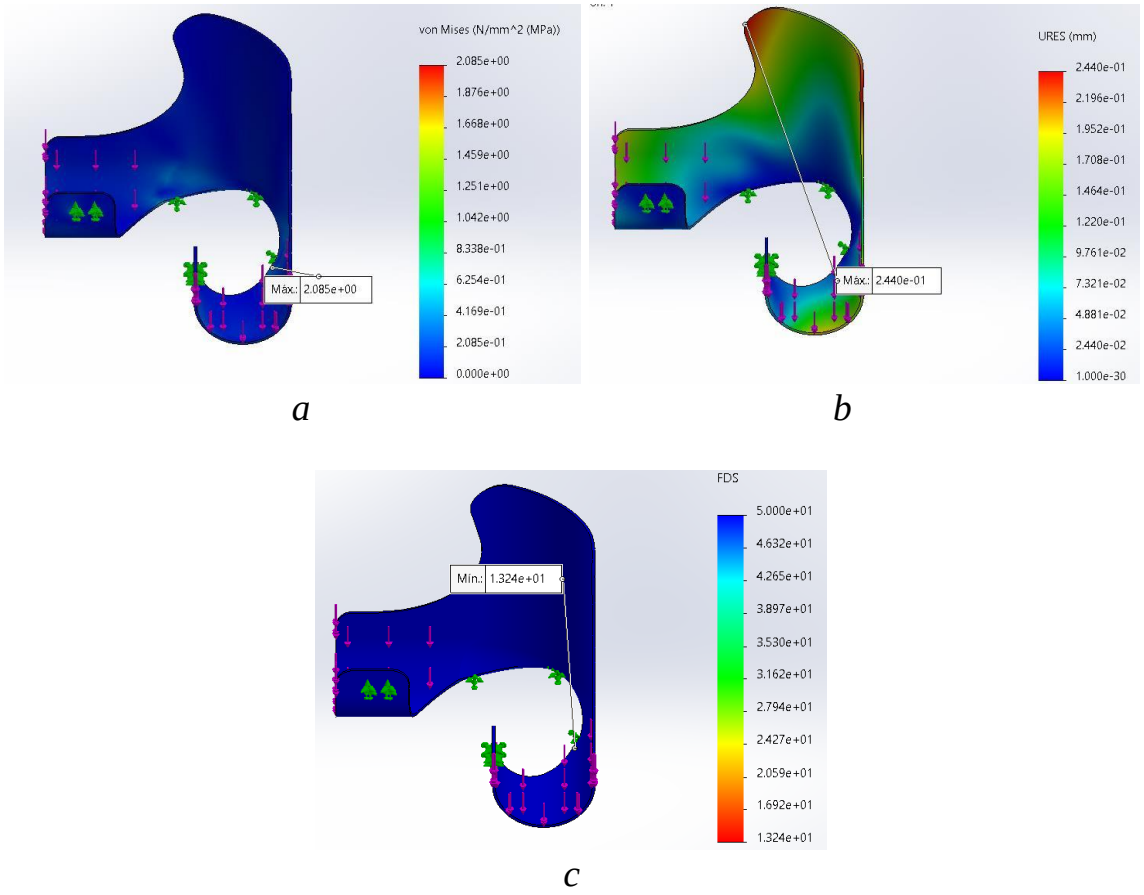

a *b*

c

Fig. 5. Finite element analysis results for vertical position: *a* – Von Mises stress; *b* – displacement; *c* – safety factor

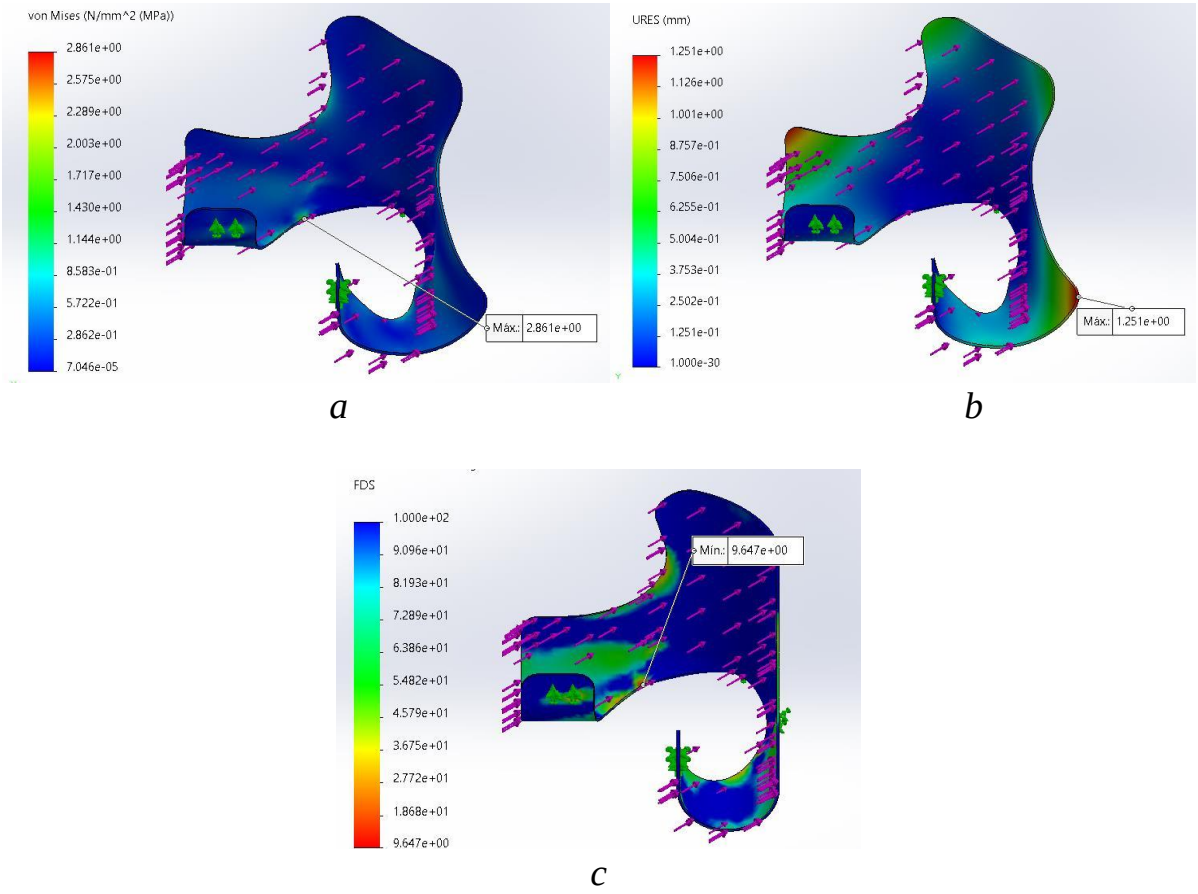

Fig. 6. Finite element analysis results for horizontal position: *a* – Von Mises stress; *b* – displacement; *c* – safety factor

Finally, Table 5 shows a comparison of the results for both critical situations, with the horizontal position identified as the situation with the greatest stress and deformation.

Table 5
Comparison of simulation results for commercial splints in horizontal and vertical positions

Parameters	Vertical position	Horizontal position
Maximum stress / safety factor	2.085 MPa / 13.24	2.861 MPa / 9.647
Maximum deformation	0.244 mm	1.251 mm

The horizontal position was identified as the critical load case, presenting the greatest stress and deformation values. This position was therefore selected for all subsequent analyses, as it represents the worst-case scenario for structural design validation.

5. 3. Minimum safety factor determination using Pugsley methodology

To determine the appropriate minimum safety factor for the abduction splint, Pugsley tables were used, which allow selecting a realistic value considering the

specific characteristics of the design and its clinical application. Fig. 7 shows the Pugsley tables used for this determination.

Characteristic			B			
			ar	Good	Good	Good
Ab	C=	mb	1.1	2.3	2.5	6.7
		b	1.2	Good	☆or	Good
		ɒ	1.5	Good	Poor	Good
		p	☆r	Good	Good	Good
Ab	C=	mb	1.3	1.55	1.3	1.45
		b	1.45	1.77	3.04	3.35
		r	6.6	1.9	1.1	6.66
		p	1.5	1.1	2.4	2.1
Ar	C=	mb	5.7	1.8	2.1	3.2
		b	1.1	2.3	2.5	2.75
		r	1.9	2.3	2.8	3.1
		ɒ	1.9	2.5	2.7	3.7
Ap	C=	Galan	1.7	2.75	2.4	3.48
		b	1.95	2.05	3.45	3.11
		Grŝun	2.4	2.35	3.1	3.55
		p	2.2	3.45	3.45	3.95
Very Good			Regular			
Very Good			== Pror			

Characteristic		D		
		ns	s	ms
E=	ns	1.0	1.2	1.4
	s	1.2	1.3	1.5
	ms	1.2	1.4	1.6
Very Serious		Serious	Not Serious	

Fig. 7. Pugsley tables used for determining the minimum safety factor

The method establishes the minimum safety factor ($SF_{\min}$) through the following relationship

$$SF_{\min} = n_s * k, \tag{6}$$

where $n_S = n_{xx} * n_{yy}$; n_{xx} – factor associated with characteristics A, B, and C (material quality, applied load control, and stress analysis accuracy); n_{yy} – factor associated with characteristics D and E (user hazard and economic impact); k – additional correction factor (k = 1.2 for pediatric medical devices).

The selected characteristics were: A (material quality): fair; B (load control): fair; C (finite element analysis accuracy): very good; D (user hazard): serious; E (economic impact): not serious.

According to Pugsley tables: For A-B-C (fair-fair-very good): n_{xx} = 2.1; For D–E (serious-not serious): n_{yy} = 1.0 → n_S = 2.1 * 1.0 = 2.1. Applying the correction factor k = 1.2

$$SF_{\min} = 2.1*1.2 = 2.52. \tag{7}$$

This minimum safety factor of 2.52 establishes the threshold for structural design validation. Any design achieving a safety factor above this value is considered structurally safe for pediatric medical device applications, providing adequate margin for manufacturing variations and unexpected loading conditions.

5. 4. Comparative finite element analysis of medical-grade materials

Static simulations were performed for three medical-grade materials suitable for fused deposition modeling additive manufacturing. Table 6 presents the materials selected for comparative analysis.

Table 6

Materials selected for static and comparative analysis in splint design

Material	*E*, GPa	Poisson	σ_{yield}, MPa	Density, g/cm^3
ABS Medical [28, 29]	1.40	0.37	46	1.06
PETG Medical [30–32]	2.20	0.40	37–39	1.27
PP [33, 34]	0.62–0.67	0.43	18–20	0.90

Fig. 8 shows the simulation results for acrylonitrile butadiene styrene medical material.

Fig. 9 shows the simulation results for polyethylene terephthalate glycol medical material.

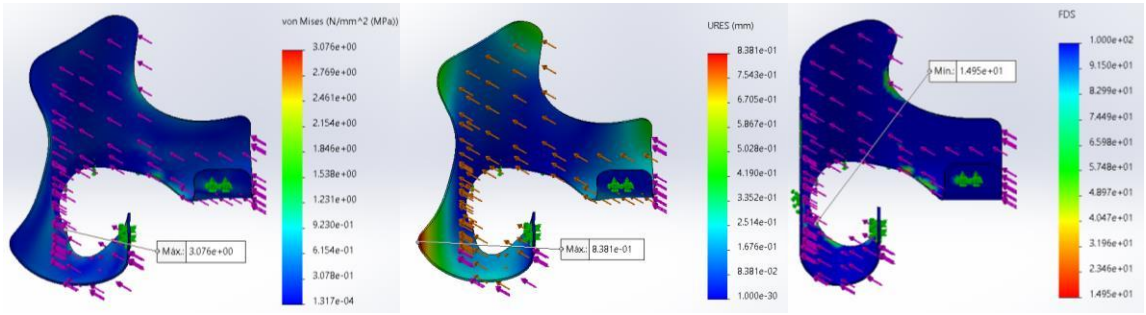

a *b* *c*

Fig. 8**.** Simulations for acrylonitrile butadiene styrene medical material: *a* – Von Mises stress; *b* – displacement; *c* – safety factor

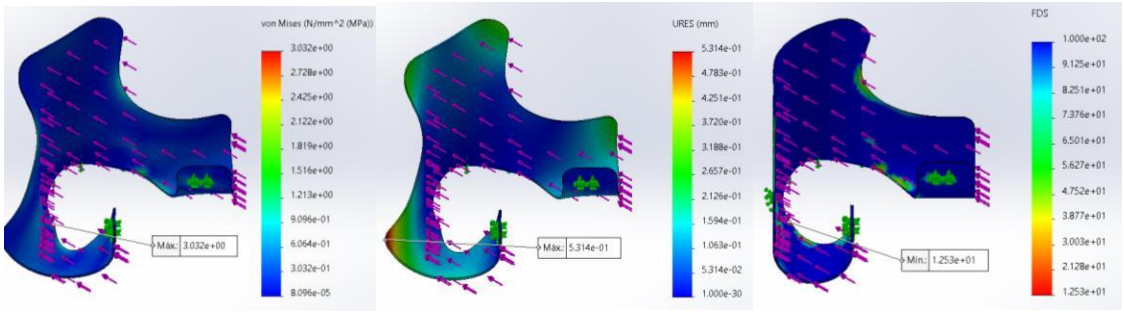

a *b* *c*

Fig. 9. Simulations for polyethylene terephthalate glycol medical material: *a* – Von Mises stress; *b* – displacement; *c* – safety factor

Fig. 10 shows the simulation results for polypropylene material.

The results of material comparison in horizontal position are summarized in Table 7.

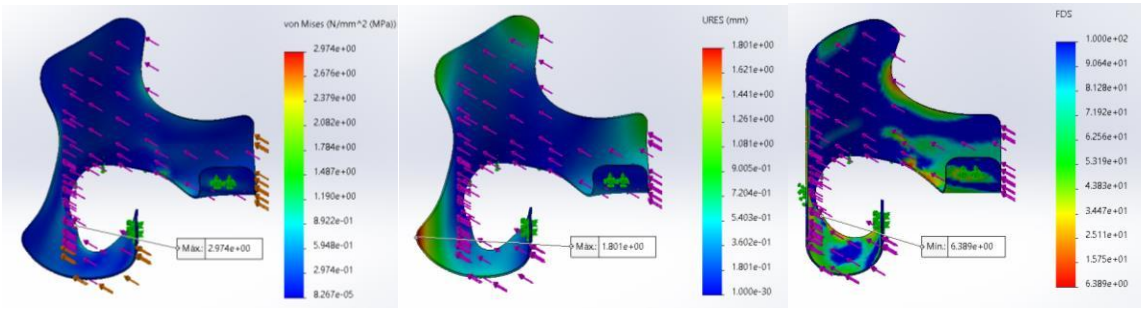

a *b* *c*

Fig. 10. Simulations for polypropylene material: *a* – Von Mises stress; *b* – displacement; *c* – safety factor

Table 7

Comparative finite element analysis results for medical-grade materials (horizontal position)

Material	*E*, GPa	σ_{yield}, MPa	σ_{max}, MPa	SF	Def., mm	Mass, g
ABS Medical	1.40	46	3.076	14.95	0.838	395.34
PETG Medical	2.20	38	3.032	12.53	0.531	473.67
PP	0.65	19	2.974	6.389	1.801	335.67

Acrylonitrile butadiene styrene medical grade was selected as the optimal material due to its high safety factor of 14.95, which exceeds the minimum required value of 2.52 by a factor of 5.9. This material provides the best balance between structural performance, manufacturability, and biocompatibility for the intended application.

5. 5. Topological optimization and design validation using solid isotropic material with penalization method

The solid isotropic material with penalization method was implemented for topological optimization. The compliance minimization objective function is

$$C = \sum \rho_e^p \cdot u_e^T \cdot K_e \cdot u_e, \quad (8)$$

where ρ_e – the element density, p – the penalization exponent (p = 3), u_e – the element displacement vector, and K_e – the element stiffness matrix.

Compliance minimization was selected as the objective function because it is mathematically equivalent to maximizing the global structural stiffness of the device. This criterion ensures that the optimized geometry retains the maximum load-bearing capacity per unit of remaining volume, which is critical for orthotic applications where deformation under load must be controlled to preserve the therapeutic abduction angle. Compared to stress-based objectives, compliance minimization offers superior numerical stability and monotonic convergence within the SIMP framework, making it the standard choice for structural topology optimization in medical device design [21, 22].

The optimization converged after 81 iterations, as shown in the convergence graphs (Fig. 11).

Fig. 12 shows the material density distribution map from the topological optimization study, where yellow regions indicate material to be retained and blue regions indicate material acceptable for removal.

Based on the optimization results, a new geometry was designed following the material distribution template. Fig. 13 shows the redesign process with dimensional overlay.

Fig. 14 shows the final optimized splint design ready for additive manufacturing.

Table 8 presents the comparison between original and optimized designs.

The results presented in Table 8 show that the topological optimization has achieved its primary objective of reducing mass while maintaining structural strength. The 18.96% reduction in volume and weight (from 395.34 g to 320.38 g) is justified by the redistribution of material, rationally established along the principal stress paths identified by the SIMP method, where low-stress zones that add weight to the element without providing any structural benefit are excluded. The corresponding 8.43% reduction in the safety factor, from 14.95 to 13.69, confirms that material has been removed only from non-critical areas, since the optimized design still exceeds the minimum of 2.52 by a factor of 5.4. The 18.33% increase in the maximum skin contact pressure value (from 0.813 kPa to 0.962 kPa), which is well below the 5.2 kPa threshold for capillary occlusion, shows that the geometric modifications introduced by the optimization do not compromise skin safety. The 15.52% reduction in the contact area indicates that peripheral material was removed from the interface between the skin and the device, while the 24.34% increase in maximum deformation, from 0.838 mm to 1.042 mm, is consistent with the reduced structural stiffness resulting from the decrease in material volume and is anatomically negligible, given its use in the treatment of DDH. The Fig. 15 shows the FEA validation results of the optimized splint design.

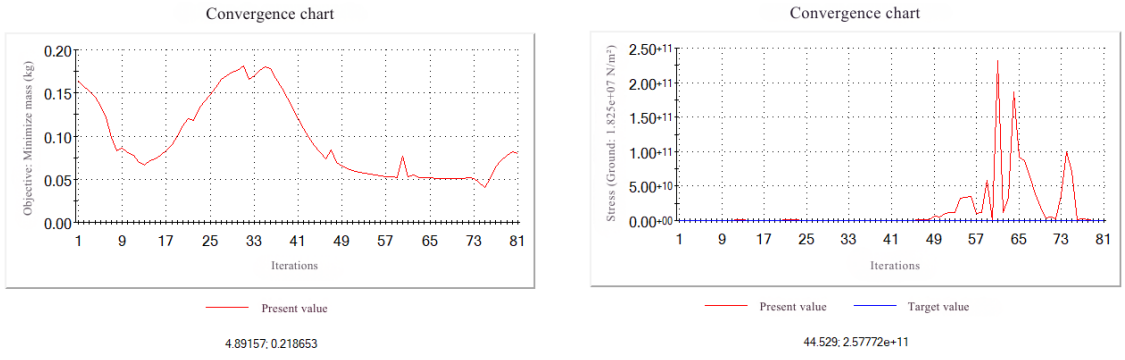

a *b*

Fig. 11. Convergence graphs: *a* – compliance convergence; *b* – volume fraction convergence

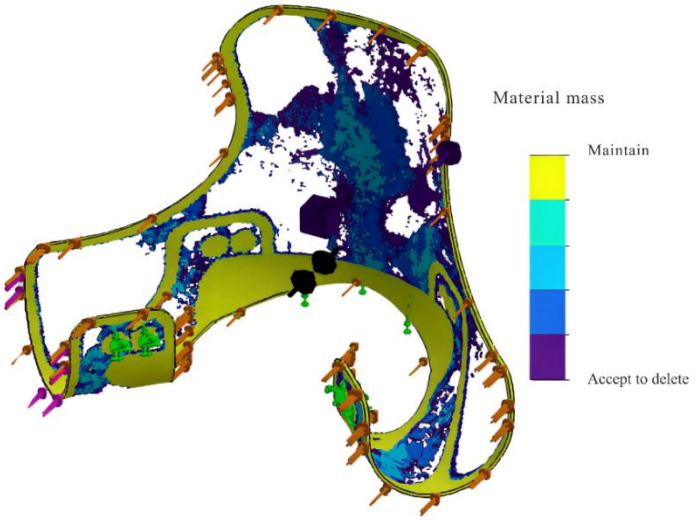

Fig. 12. Topological optimization results showing material density distribution: yellow regions indicate material to be retained, blue regions indicate material acceptable for removal

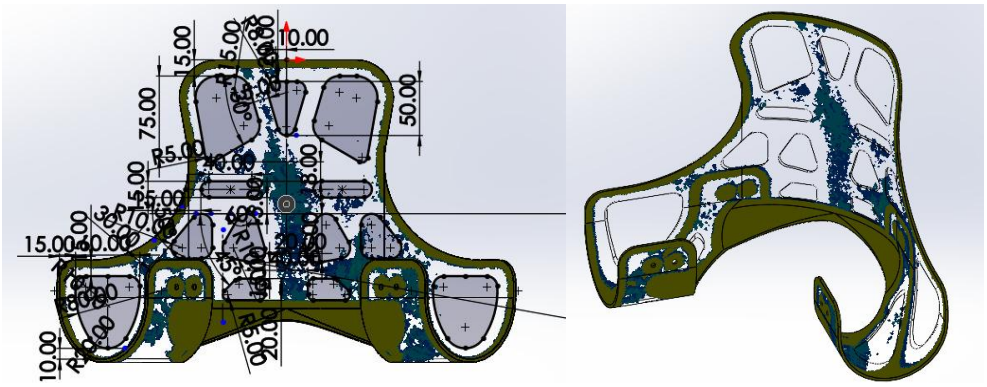

a *b*

Fig. 13. Redesign process: dimensional overlay on optimization results for manufacturing guidance: *a* – sketch on the body for cutting material; *b* – result of cutting the material

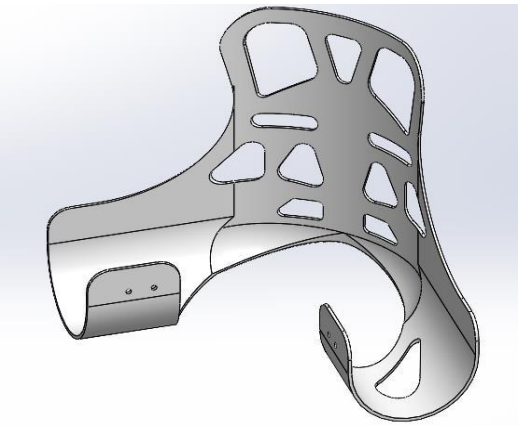

Fig. 14. Final design of optimized abduction splint with topologically derived cutouts for weight reduction while maintaining structural load paths

Table 8
Comparison between original and topologically optimized designs

Parameter	Original	Optimized	Variation (%)
Volume (mm^3)	373,056.26	302,249.70	-18.96
Mass (g)	395.34	320.38	-18.96
Maximum effort. (MPa)	3.076	3.359	+9.20
Maximum deformation (mm)	0.838	1.042	+24.34
Safety factor (FS)	14.95	13.69	-8.43
Contact area (mm^2)	121,107.78	102,309.49	-15.52
Maximum contact pressure (kPa)	0.813	0.962	+18.33

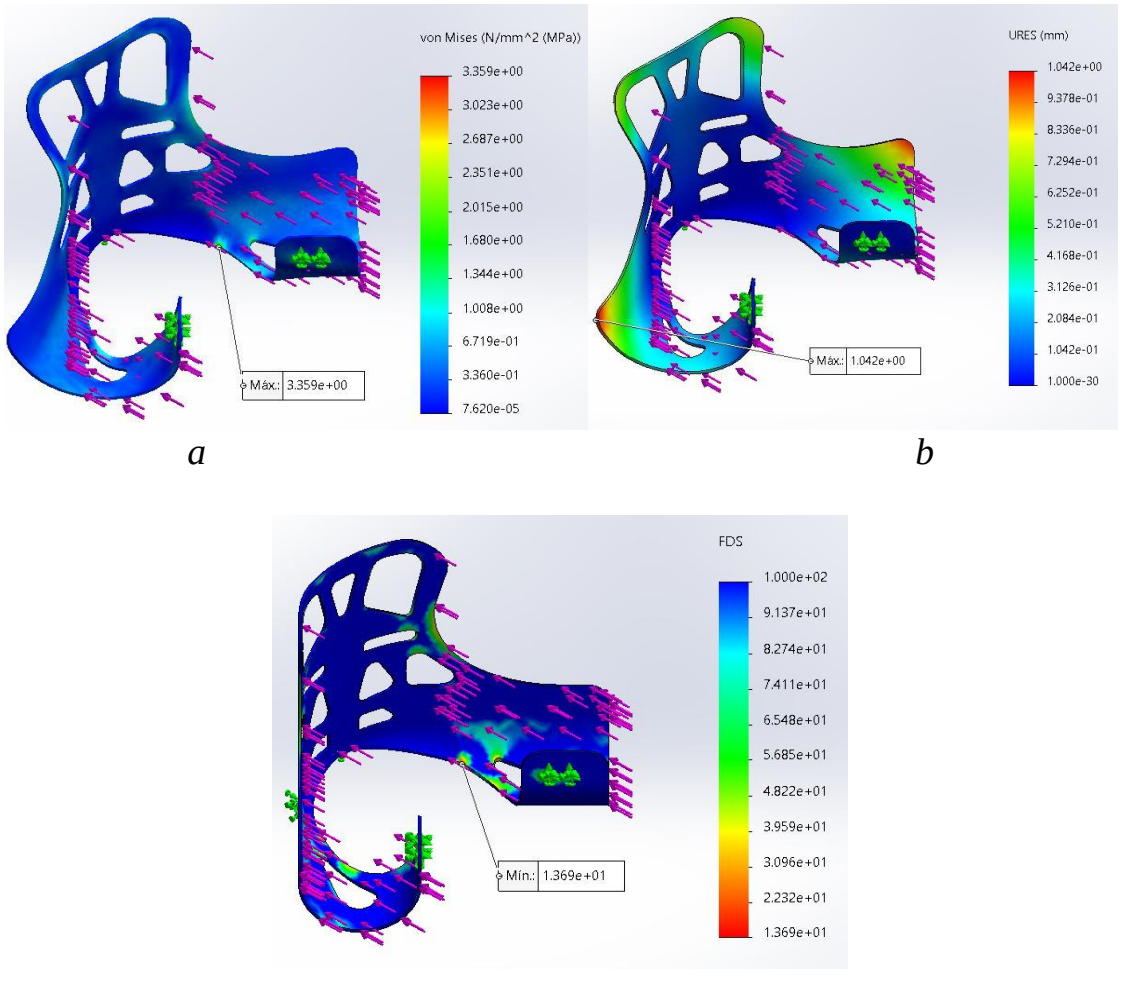

a *b*

c

Fig. 15. Finite element analysis **(**FEA) validation of the optimized design: *a* – Von Mises stress distribution (max. 3,359 MPa, elastic limit 46 MPa indicated); *b* – displacement field (max. 1,042 mm); *c* – safety factor distribution (min. SF = 13.69)

Finally, a comparison was made of the characteristics from the original PP Copolymer splint, the splint with static analysis of medical ABS, and the latter with topological optimization as shown in Table 9.

The maximum contact pressure in the optimized design was 0.962 kPa, significantly below the 5.2 kPa threshold for capillary closing pressure. The

optimized design maintains contact pressure at 18.5% of the critical threshold, ensuring safe conditions that prevent tissue ischemia and pressure ulcer development.

The topological optimization process achieved an 18.96% reduction in volume and mass (from 395.34 g to 320.38 g), while maintaining a safety factor of 13.69, which is 5.4 times higher than the minimum required value of 2.52 established using Pugsley methodology. These results demonstrate that the optimization successfully reduced device weight while preserving structural integrity and ensuring safe contact pressure levels for pediatric patients.

Table 9
Comparison of results for original and optimized splints

Characteristic	Original splint	Designed splint	Optimized splint
Material	PP Copolimero	ABS Medical	ABS Medical
Volume (mm^3)	372,964.66 mm^3	372,964.66 mm^3	302,249.70 mm^3
Mass (g)	395.34 g	395.34 g	320.38 g
Maximum deformation (mm)	1.251 mm	0.838 mm	1.042 mm
Maximum effort. (MPa)	2.861 MPa	3.076 MPa	3.359 MPa
Safety factor (FS)	9.65	14.95	13.69
Contact area (mm^2)	121,107.78 mm^2	121,107.78 mm^2	102,309.49 mm^2
Maximum contact pressure (kPa)	0.813 kPa	0.813 kPa	0.962 kPa

6. Discussion of topological optimization results for abduction splint design

The topological optimization process achieved an 18.96% mass reduction (from 395.34 g to 320.38 g), as shown in Table 8. This result is explained by the optimal redistribution of material along the principal stress paths identified through finite element analysis. The solid isotropic material with penalization method, with penalization exponent $p = 3$ (8), effectively forced intermediate density elements to converge toward discrete values of zero or one, resulting in a clearly defined geometry suitable for additive manufacturing. The convergence graphs in Fig. 11 demonstrate that the optimization reached stability after 81 iterations, indicating that the solution represents a true optimum rather than a local minimum.

The selection of acrylonitrile butadiene styrene medical grade as the optimal material is justified by the comparative finite element analysis results presented in Table 7. This material achieved a safety factor of 14.95, compared to 12.38 for polyethylene terephthalate glycol and 6.03 for polypropylene. After topological optimization, the safety factor decreased to 13.69 (Fig. 15, *c*), which still exceeds the minimum required value of 2.52 (7) by a factor of 5.4. This substantial margin accommodates manufacturing variations inherent to fused deposition modeling processes, where layer adhesion and printing parameters can affect mechanical properties.

The contact pressure validation of 0.962 kPa represents a critical finding for pediatric patient safety. This value is significantly below the 5.2 kPa threshold for capillary occlusion established in the biomechanical literature [20, 23, 24], maintaining contact pressure at only 18.5% of the critical threshold. The low contact pressure is explained by the increased contact surface area resulting from the optimized geometry, which distributes loads more uniformly across the skin-device interface.

The increase in maximum deformation from 0.838 mm to 1.042 mm (Table 9) is explained by the reduced structural stiffness resulting from material removal. However, this 24.34% increase in deformation remains within acceptable limits, as the magnitude is negligible compared to the anatomical tolerances involved in developmental dysplasia of the hip treatment, where therapeutic positioning requires angular ranges of several degrees.

The 18.96% mass reduction achieved in this study compares favorably with similar topological optimization applications in orthopedic devices. The research presented in [23] reported a 9.58% mass reduction in orthoses for fractures using multicriteria material selection combined with topological optimization. The present study achieved almost double this improvement, which can be attributed to the specific geometry of abduction splints that offers greater potential for material redistribution compared to more compact orthotic devices.

The work in [22] applied topological optimization to upper limb orthoses, achieving improved comfort and reduced weight through integration with 3D printing. However, specific quantitative mass reduction values were not reported, limiting direct numerical comparison. The study in [24] demonstrated successful application of topological optimization to anthropomorphic prosthetic limbs using plantogram-derived pressure data, achieving improved pressure distribution similar to the contact pressure optimization obtained in the present study.

A distinctive feature of this study is the combined validation of three critical parameters: mass reduction (18.96%), structural safety (SF = 13.69), and contact pressure (0.962 kPa). Previous optimization studies typically focused on only one or two of these factors. Furthermore, the application of Pugsley's methodology (6), (7) to establish the minimum SF (Fig. 8) provides a rigorous foundation for safety, moving beyond the arbitrary values commonly cited in orthotic design.

The finite element model assumes linear elastic, isotropic, and homogeneous material behavior, which does not capture the layer-dependent anisotropy introduced by the fused deposition modeling process. In practice, printed specimens exhibit lower stiffness and yield strength in the build direction, meaning the effective safety factor of the manufactured device may be lower than the simulated value.

The reference geometry was derived through reverse engineering of a commercial device. The optimization redistributes the material of the existing structure but does not correct the original design decisions, such as the location of the load-bearing section or the curvature of the leg support. If the reference device exhibits characteristics other than contact pressure and mass – such as an insufficient range of abduction or poor anatomical conformity – these limitations are carried over to the optimized design and cannot be resolved through topological optimization alone.

The study was conducted using a single anthropometric profile representing a 7-month-old female infant weighing 7.6 kg. The optimized geometry is therefore not directly transferable to patients with significantly different body proportions without repeating the full optimization process. Furthermore, the absence of physical prototyping and clinical testing means that therapeutic efficacy, caregiver usability, and skin lesion outcomes have not been verified in a real patient population, which is necessary before any clinical implementation.

Future development of this study could advance in the following directions:

– development of a parametric design system that automatically adjusts the dimensions of the splint based on the patient's anthropometric measurements. This would allow the manufacture of customized devices for each patient. The anticipated difficulty is establishing reliable correlations between external anthropometric measurements and internal anatomical structures relevant to therapeutic positioning;

– implementation of multi-objective optimization that simultaneously minimizes mass, contact pressure, and manufacturing cost while maximizing structural safety. The mathematical difficulty lies in defining the appropriate weighting factors for the conflicting objectives and ensuring Pareto-optimal solutions;

– extension to dynamic analysis incorporating infants' movement patterns and scenarios of manipulation by caregivers. The methodological challenge lies in characterizing representative dynamic load profiles for the various activities that occur during the 12- to 24-week treatment periods;

– clinical trials to validate therapeutic efficacy and compare results with conventional devices. Anticipated challenges include patient selection, ethical approval processes, long-term follow-up requirements, and establishing appropriate outcome metrics for comparative evaluation.

7. Conclusions

1. Biomechanical force calculation based on pediatric anthropometric data established that a 7-month-old infant with body weight of 7.6 kg generates forces of 11.93 N per leg and moments of 1.79 Nm on the abduction splint structure. The horizontal position was identified as the critical load case, presenting 29.6% higher stress values compared to the vertical position. These results are explained by the increased moment arm in horizontal orientation, where gravitational forces act perpendicular to the splint structure. This biomechanical characterization provides validated input parameters for finite element analysis of pediatric orthotic devices, addressing the absence of specific load data for abduction splints in the existing literature.

2. Mechanical design through reverse engineering of a commercial device established a validated baseline geometry with mass of 406.56 g and safety factor of 9.647 in the critical horizontal position. The computer-aided design model accurately reproduced the functional features of clinical abduction splints, including bilateral leg supports, pelvic section, and angular adjustment mechanism. This baseline design enabled systematic comparison between original and optimized configurations, demonstrating that commercial devices exceed minimum structural requirements but present opportunities for mass optimization without compromising safety.

3. Minimum safety factor determination using Pugsley methodology established a threshold of 2.52 for structural design validation of pediatric medical devices. This value was calculated considering fair material quality, fair load control, very good analysis accuracy, serious user hazard, and not serious economic impact, with an additional correction factor of 1.2 for pediatric applications. Unlike arbitrary safety factor selection common in similar studies, this systematic approach provides documented justification based on specific design characteristics and clinical

application requirements, ensuring adequate margins for manufacturing variations and unexpected loading conditions.

4. Comparative finite element analysis of three medical-grade materials identified acrylonitrile butadiene styrene medical grade as optimal, achieving a safety factor of 14.95 compared to 12.38 for polyethylene terephthalate glycol and 6.03 for polypropylene. This superior performance is explained by the favorable combination of yield strength (46 MPa) and elastic modulus (1.40 GPa), which provides adequate stiffness for therapeutic positioning while maintaining substantial safety margins. The selected material exceeds the minimum required safety factor by 5.9 times, accommodating the property variations inherent to fused deposition modeling additive manufacturing processes.

5. Topological optimization using the solid isotropic material with penalization method achieved an 18.96% mass reduction (from 395.34 g to 320.38 g) while maintaining structural integrity with a safety factor of 13.69 and contact pressure of 0.962 kPa. The optimization converged after 81 iterations with penalization exponent $p = 3$, demonstrating stable solution convergence. This mass reduction nearly doubles the 9.58% achieved in similar orthopedic device optimization studies, which is explained by the specific geometry of abduction splints that offers greater potential for material redistribution. The contact pressure of 0.962 kPa represents only 18.5% of the 5.2 kPa capillary occlusion threshold, effectively addressing the skin lesion concerns documented as primary barriers to treatment compliance in developmental dysplasia of the hip management.

Conflict of Interest

The authors declare that they have no conflict of interest in relation to this study, whether financial, personal, authorship or otherwise, that could affect the study and its results presented in this paper.

Financing

This study was conducted entirely with the authors' own resources and received no grants or financial support from public or private entities.

Data availability

The datasets generated and analyzed during the current study are available from the corresponding author on reasonable request.

Use of artificial intelligence

The authors confirm that no artificial intelligence tools were used in the preparation of this manuscript for text generation, data analysis, or figure design.

Acknowledgements

The research team is grateful to the Professional School of Mechanical Engineering at the National University of San Agustin de Arequipa for providing access to the facilities and equipment required to carry out this project.

Author Contributions

Alex Condori: Conceptualization, Methodology, Design, Research, Writing – Original Draft; **Eber Mejia**: Validation, Supervision, Project Management, Writing – Review and Editing; **Yuri L. Silva**: Review and Corrections; **Erick Valdeiglesias Flores**: Research, Translation; **Daniela Ponte**: Research, Analysis of Results; **Trunks Giorgio Vásquez Llave**: Research, Data Curation.

References

1. Ionescu, A., Dragomirescu, M.-C., Herdea, A., Ulici, A. (2023). Developmental Dysplasia of the Hip: How Many Risk Factors Are Needed? Children, 10 (6), 968. https://doi.org/10.3390/children10060968

2. Burden of Disease. Global Hip Dysplasia Registry. Available at: https://www.hipregistry.com/burden-of-disease

3. Tao, Z., Wang, J., Li, Y., Zhou, Y., Yan, X., Yang, J. et al. (2023). Prevalence of developmental dysplasia of the hip (DDH) in infants: a systematic review and meta-analysis. BMJ Paediatrics Open, 7 (1), e002080. https://doi.org/10.1136/bmjpo-2023-002080

4. Kraus, T., Chiari, C. (2024). Universal screening for developmental dysplasia of the hip in Austria: what have we learned? Exploration of Musculoskeletal Diseases, 2 (3), 208–215. https://doi.org/10.37349/emd.2024.00049

5. Talal Ahmad Amer, M.D., A. R. M. M. D., Elaziz Elsaaid, M.D., M. A. (2021). Role of Ultrasound in Screening of Infantile Developmental HipDysplasia. The Medical Journal of Cairo University, 89 (3), 329–336. https://doi.org/10.21608/mjcu.2021.153946

6. Hip dysplasia. Mayo Clinic. Available at: https://www.mayoclinic.org/diseases-conditions/hip-dysplasia/symptoms-causes/syc-20350209

7. Guías de Salud. Available at: https://www.lne.es/salud/guia/

8. Jacobsen, K. K., Laborie, L. B., Kristiansen, H., Schäfer, A., Gundersen, T., Zayats, T., Rosendahl, K. (2024). Genetics of hip dysplasia – a systematic literature review. BMC Musculoskeletal Disorders, 25 (1). https://doi.org/10.1186/s12891-024-07795-2

9. Pavone, V., de Cristo, C., Vescio, A., Lucenti, L., Sapienza, M., Sessa, G. et al. (2021). Dynamic and Static Splinting for Treatment of Developmental Dysplasia of the Hip: A Systematic Review. Children, 8 (2), 104. https://doi.org/10.3390/children8020104

10. Drobniewski, M., Gonera, B., Olewnik, Ł., Borowski, A., Ruzik, K., Triantafyllou, G., Borowski, A. (2024). Challenges and Long-Term Outcomes of Cementless Total Hip Arthroplasty in Patients Under 30: A 24-Year Follow-Up Study with a Minimum 8-Year Follow-Up, Focused on Developmental Dysplasia of the Hip. Journal of Clinical Medicine, 13 (21), 6591. https://doi.org/10.3390/jcm13216591

11. O'Brien, M. J., Semciw, A. I., Mechlenburg, I., Tønning, L. C., Stewart, C. J., Kemp, J. L. (2023). Pain, function and quality of life are impaired in adults undergoing periacetabular osteotomy (PAO) for hip dysplasia: a systematic review

and meta-analysis. HIP International, 34 (1), 96–114. https://doi.org/10.1177/11207000231179610

12. Gahleitner, M., Pisecky, L., Gotterbarm, T., Högler, W., Luger, M., Klotz, M. C. (2023). Long-term Results of Developmental Hip Dysplasia Under Therapy With Pavlik Harness. Journal of Pediatric Orthopaedics, 44 (3), 135–140. https://doi.org/10.1097/bpo.0000000000002575

13. Rastogi, P., Anant, S., Agarwal, S., Singh Oberoi, I., Tiwari, P. (2025). A Systematic Review on Neonatal Screening and Orthopaedic Management of Developmental Dysplasia of The Hip Through a Synthesis of Diagnostic Yield and Pavlik Harness Outcomes. Journal of Neonatal Surgery, 14 (8S), 968–979. Available at: https://www.jneonatalsurg.com/index.php/jns/article/view/5223

14. Imerci, A., Thacker, M. M., Bowen, J. R. (2024). Failure of Pavlik Harness Treatment in Infants Under 6 Months Old with Dislocated Hips: Short- and Intermediate-Term Results of Subsequent Treatment Modalities. Indian Journal of Orthopaedics, 58 (9), 1288–1296. https://doi.org/10.1007/s43465-024-01162-y

15. Rakotonandrianina, M. N. H., MG., A. T. R., Tata, T. J. F., Solofomalala, G. D. (2023). Orthosis Treatment for Patients with Congenital Hip Dislocation. Surabaya Physical Medicine and Rehabilitation Journal, 5 (1), 17–24. https://doi.org/10.20473/spmrj.v5i1.36926

16. Zhi, X., Xiao, X., Wan, Y., Wei, P., Canavese, F., Xu, H. (2021). Tübingen hip flexion splint for the treatment of developmental dysplasia of the hip in children younger than six months age: A meta-analysis. Journal of Children's Orthopaedics, 15 (4), 402–408. https://doi.org/10.1302/1863-2548.15.210015

17. Wahlen, R., Zambelli, P.-Y. (2015). Treatment of the Developmental Dysplasia of the Hip with an Abduction Brace in Children up to 6 Months Old. Advances in Orthopedics, 2015, 1–6. https://doi.org/10.1155/2015/103580

18. Dyskin, E., Ferrick, M. (2015). Semirigid Abduction Bracing is Effective Treatment of Reducible Developmental Dysplastic Hips after Failure of Pavlik Harness. Ann. Orthop. Rheumatol., 3 (2), 1045. Available at: https://www.jscimedcentral.com/jounal-article-pdf/Annals-of-Orthopedics-and-Rheumatology/orthopedics-3-1045.pdf

19. Hoopes, R. R. (2020). A Retrospective Study to Identify Factors Contributing to Pressure Ulcers in Pediatric Patients with Lower Extremity Splints. Biomedical Journal of Scientific & Technical Research, 30 (3). https://doi.org/10.26717/bjstr.2020.30.004957

20. Grzybowski, G., Bliven, E., Wu, L., Schaeffer, E. K., Gibbard, M., Zomar, B. O. et al. (2022). Caregiver Experiences Using Orthotic Treatment Options for Developmental Dysplasia of the Hip in Children. Journal of Pediatric Orthopaedics, 43 (2), 105–110. https://doi.org/10.1097/bpo.0000000000002312

21. Sala, F., D'Urso, G. D., Giardini, C. (2024). Evaluation of the Integration of Topological Optimisation in the Process Chain for Manufacturing Customised Orthopaedic Devices via Additive Manufacturing. Prosthesis, 6 (6), 1510–1528. https://doi.org/10.3390/prosthesis6060109

22. Voulgaris, S., Kousiatza, C., Kazakis, G., Ypsilantis, K.-I., Galanis, D., Mitropoulou, C. Ch. et al. (2025). Upper Limb Orthoses: Integrating Topology

Optimization and 3D Printing for Custom Fit and Function. Applied Sciences, 15 (2), 827. https://doi.org/10.3390/app15020827

23. Salazar Loor, R. B., Martínez-Gómez, J., Sarmiento Anchundia, J. (2025). Material Selection for the Development of Orthoses Using Multicriteria Methods (MCDMs) and Simulation. Processes, 13 (6), 1796. https://doi.org/10.3390/pr13061796

24. Kyriakidis, I. F., Kladovasilakis, N., Gavriilopoulos, M., Tzetzis, D., Pechlivani, E. M., Tsongas, K. (2025). Topologically Optimized Anthropomorphic Prosthetic Limb: Finite Element Analysis and Mechanical Evaluation Using Plantogram-Derived Foot Pressure Data. Biomimetics, 10 (5), 261. https://doi.org/10.3390/biomimetics10050261

25. Raimann, R., Aguirre, D. (2021). Displasia del desarrollo de la cadera: tamizaje y manejo en el lactante. Revista Médica Clínica Las Condes, 32 (3), 263–270. https://doi.org/10.1016/j.rmclc.2021.04.003

26. Legorreta Cuevas, J. G. (2013). Mediciones básicas en displasia del desarrollo de la cadera. Rev. Mex. Ortop. Pediatr., 15 (1), 53–56. Available at: https://www.medigraphic.com/pdfs/opediatria/op-2013/op131j.pdf

27. Estimacion del peso ideal en sujetos amputados (Plamp). FRESENIUS KABI. Available at: https://www.nutricionemocional.es/sites/default/files/estimacion_peso_ideal_sujetos_amputados_1.pdf

28. ABS Medical (Technical datasheet v2.1). Weerg. Available at: https://www.weerg.com/hubfs/Datasheets/Datasheets%202024/ENG/EN_ABSMedical.pdf

29. Zou, R., Xia, Y., Liu, S., Hu, P., Hou, W., Hu, Q., Shan, C. (2016). Isotropic and anisotropic elasticity and yielding of 3D printed material. Composites Part B: Engineering, 99, 506–513. https://doi.org/10.1016/j.compositesb.2016.06.009

30. Ciganas, J., Janušas, G. (2023). Investigation of Dynamic Mechanical Properties of PETG Thermoplastic. In Proc. 27th Int. Sci. Conf. MECHANICS, Kaunas University of Technology, Kaunas, Lithuania. Available at: https://mechanic.ktu.edu/wp-content/uploads/sites/296/2023/05/P.5.pdf

31. PETG. Technical Data Sheet 05.24. AZUREFILM. Available at: https://3d.nice-cdn.com/upload/file/TDS-PETG.pdf

32. PETG (Technical Data). PETG. PT Polimer Tecnic. Available at: https://www.polimertecnic.com/wp-content/uploads/2022/05/1H9L9sb0yOuoFQIHCREpQda92QUpMetsC.pdf

33. Technical data sheet: P-filament. PP Print. Available at: https://www.ppprint.de/wp-content/uploads/2019/03/PPprint-data-sheet-eng-21.02.2019.pdf

34. Yun, J.-H., Jeon, Y.-J., Kang, M.-S. (2022). Analysis of Elastic Properties of Polypropylene Composite Materials with Ultra-High Molecular Weight Polyethylene Spherical Reinforcement. Materials, 15 (16), 5602. https://doi.org/10.3390/ma15165602